Available online at www.sciencedirect.com
ScienceDirect
International Journal of Heat and Mass Transfer 50 (2007) 4141–4150
International Journal of HEAT and MASS TRANSFER
www.elsevier.com/locate/ijhmt

Constructal cooling channels for micro-channel heat sinks

T. Bello-Ochende *, L. Liebenberg, J.P. Meyer

Department of Mechanical and Aeronautical Engineering, University of Pretoria, 0002 Pretoria, South Africa

Received 7 September 2006; received in revised form 26 February 2007
Available online 20 April 2007

Abstract

This paper documents the geometric optimisation of a three-dimensional micro-channel heat sink. The objective is to minimise the peak temperature from the walls to the coolant fluid. The optimisation is performed numerically by using the finite volume method. The numerical simulation was carried out on a unit cell with volume ranging from 0.1 mm^3 to 0.9 mm^3 and pressure drop between 10 kPa and 75 kPa. The axial length of the micro-channel heat sink was fixed at 10 mm. The cross-sectional area of the micro-channel heat sink is free to morph with respect to the degree of freedoms provided by the aspect ratio and the solid volume fraction. The effect of the total solid volume fraction and the pressure drop on the aspect ratio, channel hydraulic diameter and peak temperature is investigated. The numerical results show that the degrees of freedom have a strong effect on the peak temperature and the maximum thermal conductance. The optimal geometric characteristics obtained numerically (the aspect ratio and the optimal channel shape (hydraulic diameter)) are reported and compared with those obtained from approximate relationships using scale analysis. The predicted trends are found to be in good agreement with the numerical results.
© 2007 Elsevier Ltd. All rights reserved.

Keywords: Constructal; Micro-channel heat sinks; Conductance; Optimal geometry

1. Introduction

The quest for better designs for the cooling of heat generating devices has been a driving force for innovation and new fundamentals for heat transfer engineering and science. Micro-channel are currently in the forefront of cooling technologies, because of the difficulties of meeting with air-cooling techniques the cooling needs of devices with high heat flux (projected to exceed 100 W/cm^2 [1–3]). In modern heat transfer, the challenge is how to cool, manufacture, decreasing cost and optimise performance. To solve these problems, several novel techniques have been proposed and studied theoretically, numerically and experimentally. A review of these techniques has been conducted by Dirker et al. [1].

With the recent development of reliable numerical packages and their easy availability, optimisation of coupled convective flow (forced and natural) and conduction heat transfer has become easier to implement, and more popular. A review of the subject has been given by Bejan [4,5], which focuses on the generation of shape and structure in freely morphing convective systems, by maximising global performance subject to global constraints. This view is known as constructal theory. An area where this theory is of utmost importance is in heat transfer augmentation [6–9] were volumes reserved for fluids that act as a heating or cooling agent are optimised.

Significant research [10–15] has also been conducted on the flow and heat transfer characteristics of micro-channel heat-sinks, because of their promise to cool areas with high heat flux. These studies relied on numerical techniques and experiments [11–19] to study the flow and heat transfer characteristics of micro-channel heat sinks.

In the present paper, starting from a basic construction unit (the elemental volume is the constructal approach), we

* Corresponding author. Tel.: +27 12 420 3105; fax: +27 12 362 5124.
E-mail address: tunde.bello-ochende@up.ac.za (T. Bello-Ochende).

0017-9310/$ - see front matter © 2007 Elsevier Ltd. All rights reserved.
doi:10.1016/j.ijheatmasstransfer.2007.02.019

Nomenclature

A	channel cross-sectional area
Be	Bejan number based on a unit volume, $\Delta PV^{2/3}/\alpha\mu$
Be_L	Bejan number based on L, $\Delta PL^2/\alpha\mu$
B	channels width
C	dimensionless global conductance
C_p	specific heat at constant pressure
D_h	hydraulic diameter
f	friction factor
G	width of computational domain $(B + t_1)$
$\bar{h}$	average heat transfer coefficient
H	height
H_c	channel height
k	thermal conductivity
L	axial length
n	normal
num	number of channels
P	pressure
P_c	perimeter of micro-channel
Po	Poiseuille number based on hydraulic diameter
Pr	Prandtl number
q	total heat transfer
q''	heat flux
R	thermal resistance
Re_{D_h}	Reynolds number based on hydraulic diameter
Re_L	Reynolds number based on L
T	temperature
$T_{w,L}$	exit temperature
T_{in}	inlet temperature
T_{max}	maximum temperature
t_1	half thickness of vertical solid
t_2	base thickness
t_3	top thickness
U	average velocity
$\vec{U}$	velocity vector
V	volume
W	heat sink width
x, y, z	Cartesian coordinates

Greek symbols

α	thermal diffusivity
Δ	difference
μ	viscosity
ν	kinematic viscosity
ρ	density
ϕ	volume fraction of solid material
τ	shear stress
Ω	interface between the solid and fluid

Subscripts

c	channel
f	fluid
h	hydraulic diameter
in	inlet
max	maximum
min	minimum
opt	optimum
out	outlet
s	solid

determine numerically the best possible geometry for a micro-channel heat sink. The total elemental volume and axial length of the micro-channel heat sink is fixed. We seek to determine the best channel dimensions and system configuration that minimises the peak temperature when the pressure difference across the elemental volume is fixed.

2. Model and mathematical formulation

Fig. 1 shows a drawing of the physical model and the computational domain for a micro-channel heat sink. Heat is supplied to a highly conductive silicon substrate with known thermal conductivity from a heating area located at the bottom of the heat sink. The heat is then removed by a fluid flowing through a number of micro-channels. Using the advantage of symmetry, we select for analysis an elemental volume (unit cell) consisting of a micro-channel and the surrounding solid, as is shown in Fig. 2. This work was based on the model of Qu and Mudawar [12] and Kawano et al. [17].

The heat transfer in the elemental volume is a conjugate problem that combines heat conduction in the solid and convective heat transfer in the liquid. The two heat transfer mechanisms are coupled through the continuity of temperature and heat flux at the interface between the fluid and the solid. The fluid with inlet temperature T_{in} is driven through the micro-channel by a fixed pressure difference $\Delta P = P(z = 0) - P(z = L)$, which is maintained between the channel inlet and outlet. The objective of the following analysis is to determine the heat transfer characteristics for a given micro-channel, and the best possible configuration (L, t_1/t_2, t_2/t_3, H/G) that corresponds to the maximal global thermal conductance, or global minimal thermal resistance.

The following assumptions were made to model the heat transfer and fluid flow in the elemental volume: the hydraulic diameter of the micro-channel under analysis is greater than 10 μm; for water, the continuum regime applies hence the Navier–Stokes and Fourier equations can still be used to describe the transport processes; steady-state conditions for flow and heat transfer; incompressible flow; the properties of the solid and fluid are constant; and the heat transfer due to radiation and natural convection is negligible. It also assumed that the number of elemental micro-channels

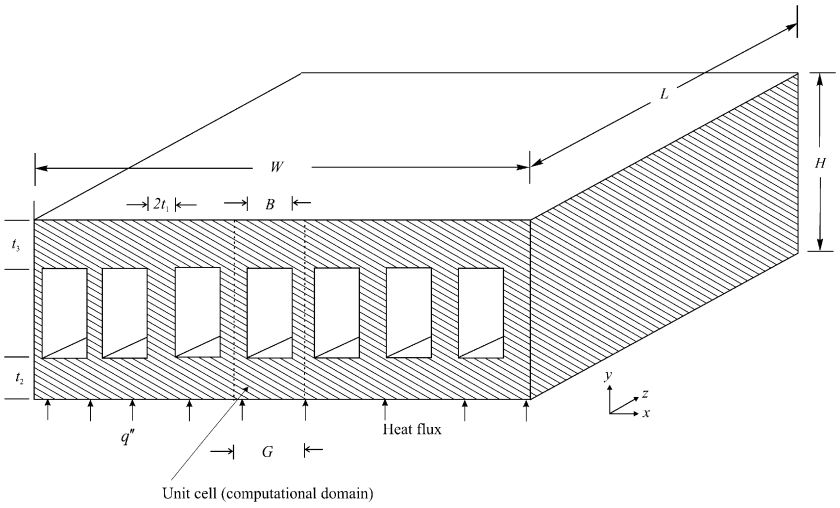

Fig. 1. Micro-channel computational unit cell of a heat sink.

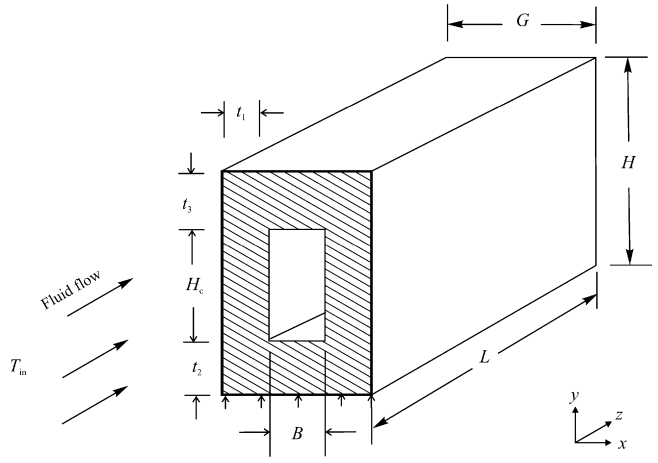

Fig. 2. Computational domain of a micro-channel heat sink.

is large. Based on these assumptions, the continuity, momentum and energy equations for the cooling fluid are

$$\nabla(\rho\vec{U}) = 0 \tag{1}$$

$$\rho(\vec{U}\cdot\nabla\vec{U}) = -\nabla P + \mu\nabla^2\vec{U} \tag{2}$$

$$\rho C_p(\vec{U}\cdot\nabla T) = k_f\nabla^2 T \tag{3}$$

where $\nabla^2 = \partial/\partial x^2 + \partial/\partial y^2 + \partial/\partial z^2$, and the origin of the Cartesian frame (x, y, z) is located in the bottom left corner of the computational domain. For the volume occupied by solid, the momentum equation is simply

$$\vec{U} = 0 \tag{4}$$

and the energy equation is

$$k_s\nabla^2 T = 0 \tag{5}$$

The entire elemental volume is treated as a continuous domain. The geometric boundary conditions for the computational domains are indicated in Fig. 2. The flow boundary conditions are such that no-slip occurs on the walls inside the channel. At the entrance of the channel, the pressure boundary conditions become

$$P = \frac{\alpha\mu Be}{V^{2/3}} + P_{\text{out}} \tag{6}$$

where Be is the dimensionless pressure drop number based on the elemental volume (the Bejan number, cf. Refs. [20,21]). $P = 1$ atm, at the channel outlet, and $T = 20$ °C at the channel inlet. The thermal boundary conditions consist of an assumed uniform heat flux that is imposed at the bottom of the heat sink

$$k_s\frac{\partial T}{\partial y} = -q'' \tag{7}$$

The remaining outside walls and the plane of symmetry of the heat sink were modelled as adiabatic. The continuity of the temperature and flux at the interface of the solid and fluid surfaces requires

$$-k_s\left.\frac{\partial T_s}{\partial n}\right|_\Omega = -k_f\left.\frac{\partial T}{\partial n}\right|_\Omega \tag{8}$$

where in each case, n is the direction normal to the wall.

The shapes of the heat sink and cooling channels are allowed to vary, by changing G, H, t_1, t_2 and t_3. We are interested in the geometric configuration that maximises the overall global thermal conductance of the geometry, which in dimensionless form is defined as

$$C = \frac{q''L}{k(T_{\max} - T_{\text{in}})} \cong \frac{q''L}{k(T_{w,L} - T_{\text{in}})} \tag{9}$$

Here q'' is the heat flux from the base of the micro-channel heat sink, k is the thermal conductivity of the fluid, and L is the length of the computational domain of the unit volume.

The global conductance C is a dimensionless way of expressing the ratio of the total heat transfer rate q divided by the largest excess temperature $(T_{w,L} - T_{in})$ reached at any point in the micro-channel heat sink. The maximum temperature is expected to occur in the exit plane of the micro-channel heat sink. The reciprocal of C is the dimensionless global thermal resistance.

3. Numerical method and code validation

The finite volume method was used to solve the continuity, momentum and energy equations. A detailed explanation is given in Patankar [22]. In the finite volume method the domain is divided into a number of control volumes such that there is one control volume surrounding each grid point. The grid point is located in the centre of the control volume. The governing equation is integrated over each control volume to derive algebraic equations containing a point value of the dependent variable at the grid point. The discretised equations express the conservation principle for a finite volume.

The second order upwind scheme was used to model the combined convection–diffusion effect in the transport equations. The resulting algebraic equations were solved using a line-by-line tri-diagonal matrix inversion algorithm. The SIMPLE algorithm [22] was then applied to solve the coupled systems of equations.

Convergence is obtained when the residuals for the mass and momentum equation are smaller than 10^{-4}, and the residual of the energy equation becomes less than 10^{-9}. A grid independence test was carried out for the micro-channel heat sink with the dimension given in Table 1. Tests show that for a control volume with a mesh size of 25 in the x-direction, 50 in the y-direction and 150 in the z-direction assures a grid independent solution in which the maximum thermal resistance changes less than 2.5% when the mesh is sequentially doubled. This mesh also guaranteed that the numerical results obtained in this work are comparable with predictions and data obtained from experimental and numerical work.

The numerical results generated were compared with the numerical results of Qu and Mudawar [12] for their case when the heating component in Fig. 1 was placed on top of the micro-channel heat sink. Fig. 3 compare the thermal resistances, R, for both the inlet and the outlet resistance. The comparison was made using the Reynolds number in the range $90 \leqslant Re_{D_h} \leqslant 400$. These parameter are defined as

$$R(x) = \frac{T(x) - T_0}{q''} \tag{10}$$

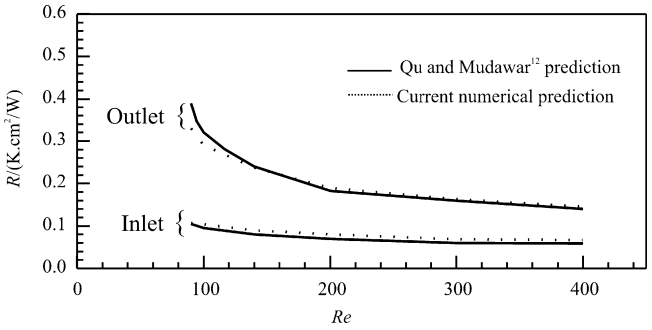

Fig. 3. Comparison of numerical predictions at inlet thermal resistance, and outlet thermal resistance.

where x is distance from the entrance, which in this case are located at $x = 0$, and $x = L$. The Reynolds number

$$Re = \frac{UD_h}{v} \tag{11}$$

and the hydraulic diameter are

$$D_h \equiv \frac{4A_c}{P_c} = \frac{4BH_c}{2(B + H_c)} = \frac{4(H - (t_2 + t_2)) \times (G - 2t_1)}{2(H + G - (2t_1 + t_2 + t_3))} \tag{12}$$

where A_c is the channel cross-sectional area and P_c is the perimeter of the micro-channel. It can be seen in Fig. 3 that the present numerical model captures the work of Qu and Mudawar [12], and it predicts very well the inlet and outlet thermal resistances. The maximum difference is 1.8% for the inlet and 1.5% for the outlet. Note also that Qu and Mudawar [12], validated their result by comparing it with the experimental data of Kawano et al. [17].

Once the model adopted in this work has been validated, numerical optimisation was conducted to determine the optimal geometry of the micro-channel using the constrained optimisation outlined in the next section. The above code verification and grid-independent test provide confidence in the numerical code used in this work.

4. Optimisation constraints and parameters

In the present work, we apply constructal theory to an arbitrary unit of micro-channel heat sink with a fixed given volume (length and cross-sectional area), and substrate material. The only parameter that is allowed to vary is the cross-sectional shape of the micro-channel heat sink, and the ratio of the internal thickness of the vertical and horizontal substrate.

The elemental volume constraint for a given computational cell is

$$GHL = V \text{ (constant)} \tag{13}$$

Table 1
Dimensions of micro-channel heat sink [12]

Case	H (μm)	G (μm)	t_1 (μm)	t_2 (μm)	$(H - (t_2 + t_3))$ (μm)	$(G - 2t_1)$ (μm)	ϕ	L (μm)
1	900	100	22.5	270	180	28	0.6638	10

and the volume of the solid substrate is

$$2Ht_1L + (G - 2t_1)Lt_2 + (G - 2t_1)t_3L = V_s \text{ (constant)} \quad (14)$$

For a fixed length we have

$$GH = \frac{V}{L} = A \text{ (constant)} \quad (15)$$

The volume of the micro-channel is therefore

$$V_f = V - V_s \text{ (constant)} \quad (16)$$

Eq. (14) can also be expressed in terms of the solid volume fraction, $\phi = V_s/V = A_s/A$. Eqs. (14)–(16) were solved simultaneously for t_1, t_2 and t_3, such that for any changes in the assumed thickness and geometric parameters, the aspect ratios (t_1/t_2, t_2/t_3, H/G and ϕ), the total volume, and volume of solid substrate remain fixed. The volume remains fixed, the cross-sectional shapes of the micro-channel heat sink change in such a way that the solid substrate conducts the heat from the base such that the thermal resistance is minimised. The total number of micro-channels in the micro-channel heat sink arrangement is obtained from

$$\text{num} = \frac{W}{B + 2t_1} \quad (17)$$

for a fixed total width, W.

5. Scale analysis and the intersection of asymptotes method

In this section, we present the use of a scaling argument to predict the optimal channel geometry that minimises the global thermal resistance or the maximum global thermal conductance. The following assumptions are made throughout the analysis: uniform flow distribution (equal flow in all the channels, constant cross-sectional area of the channels, and no inlet or exit plenum losses), the Prandtl number range $Pr > 0.5$, negligible axial conduction, and the thermal conductivity of the solid substrate is much greater than that of the fluid. The existence of an optimal arrangement can be expected based on the trade-off demonstrated in the forced convection cooling of electronics packages [8], and the method outlined by Muzychka [23]. To determine the optimal channel dimensions we use the method of intersections of asymptotes [7] for a unit micro-channel as shown in Fig. 2. The global thermal conductance scales are evaluated in two extreme limits (small channel and large channels).

The method of intersections of the asymptotes outlined by Muzychka [23] is used for determining the optimal duct shape. In the limit of small channels, the micro-channel length is covered mainly by fully developed flow and the flow is mainly Hagen–Poiseuille flow, the maximum temperature difference occurs between the outlet wall and the inlet temperature of the micro-channel heat sink. Assuming the total heat generated at the base of the micro-channel is conducted and deposited as heat current at the inner surface of the duct, the total heat transfer for a small duct for fully developed flow gives

$$q_{\text{small}} = \rho A_c U C_p (T_{w,L} - T_{in}) \quad (18)$$

where U is the average velocity defined as

$$U = \frac{A_c \Delta P D_h}{\mu P_c L Po} \quad (19)$$

Po is the Poiseuille number based on hydraulic diameter, and $Po = fRe_{D_h}/2$, therefore Eq. (18) reduces to

$$q_{\text{small}} = (T_{w,L} - T_{in}) \frac{\rho C_p A_c^2 \Delta P D_h}{\mu P_c L Po} \quad (20)$$

The resulting expression for the total heat transfer is

$$q_{\text{small}} = k_f (T_{w,L} - T_{in}) \frac{A_c^2}{P_c} \frac{D_h}{L^3} \frac{Be_L}{Po} \quad (21)$$

Be_L is the Bejan number based on the channel length ($Be_L = \Delta P L^2/\alpha\mu$). The resulting expression for dimensionless global thermal conductance is

$$C_{\text{small}} = 0.25 \frac{D_h^2}{L V^{1/3}} \frac{Be}{Po} \quad (22)$$

The above expression shows that for small channel the dimensionless thermal conductance, C_{small} is directly proportional to D_h^2.

In the opposite extreme, for large channels the flow is essentially a boundary layer flow, and the maximum temperature difference across the thermal boundary layer is given by

$$q_{\text{large}} = \bar{h} L P_c (T_{w,L} - T_{in}) \quad (23)$$

$$\bar{h} L \cong 0.453 k_f Pr^{1/3} Re_L^{1/2} \quad (0.5 < Pr < 10) \quad (24)$$

where

$$Re_L = \frac{U_\infty L}{\nu} \quad (25)$$

The core velocity U_∞ serves as the free stream velocity for the boundary layer. This velocity follows from the longitudinal pressure force balance on the control volume inscribed inside one channel

$$\Delta P A_c \cong \bar{\tau} P_c L \quad (26)$$

where $\bar{\tau}$ is the mean wall shear stress is obtained from the boundary layer solution referenced over the length L

$$\bar{\tau} = 0.664 \rho U_\infty^2 Re_L^{-1/2} \quad (27)$$

Finally, combining Eqs. (25)–(27) yields

$$Re_L = \left(\frac{\Delta P A_c L}{0.664 \rho \nu^2 P_c} \right)^{2/3} \quad (28)$$

Putting Eq. (28) into Eq. (23), the total heat transfer becomes

$$q_{\text{large}} \cong 0.5192 k_f (T_{w,L} - T_{in}) \left(\frac{\Delta P A_c P_c^2 L}{\rho \nu^2} \right)^{1/3} Pr^{1/3} \quad (29)$$

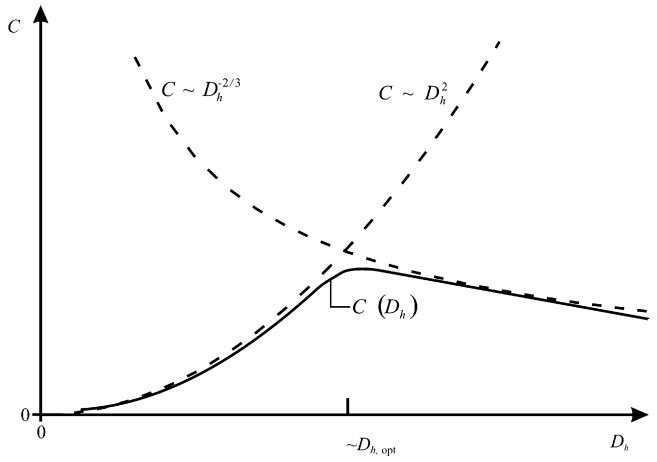

Fig. 4. The global thermal conductance in the limit of large channel/duct and small channel and the asymptote method.

or in terms of Be_L,

$$q_{\text{large}} \cong 0.5192 k_{\text{f}}(T_{\text{w},L} - T_{\text{in}})\left(\frac{A_{\text{c}}P_{\text{c}}^2}{L}\right)^{1/3} Be_L^{1/3} \tag{30}$$

In dimensionless form the global thermal conductance becomes

$$C_{\text{large}} = 1.31\frac{V^{1/9}L^{1/3}}{D_{\text{h}}^{2/3}}Be^{1/3} \tag{31}$$

The above expression shows that, C_{large} is directly proportional to $D_{\text{h}}^{-2/3}$. The dimensionless version of the equations obtained in the two limits, Eqs. (22) and (31), are reported in Fig. 4. The optimal channel shape can be approximated as the D_{h} value where the two curve intersect

$$D_{\text{h,opt}} \approx 1.86(L^3V)^{1/6}Po^{3/8}Be^{-1/4} \tag{32}$$

Po can be approximated using a single-term approximation for the Poiseuille number [24,25] for $H_{\text{c}} > B$

$$Po = \frac{12}{\left(1+\frac{B}{H_{\text{c}}}\right)^2\left[1-\frac{192}{\pi^5}\frac{B}{H_{\text{c}}}\tanh\left(\frac{\pi}{2}\frac{H_{\text{c}}}{B}\right)\right]} \tag{33}$$

Eq. (32) can be introduced in Eq. (22) or Eq. (31) to determine the maximum dimensionless global thermal conductance

$$C_{\text{max, theoretical}} \approx 0.864\frac{Be^{1/2}}{Po^{1/4}} \tag{34}$$

As shown above, the intersection of asymptotes method and scale analysis are powerful tools that allows engineers and scientists to estimate trends and optimal configurations (see Ref. [7]), preface. It is important though to understand the limits of the theoretical results obtained from Eqs. (32) and (34). There are only rough estimates of the results and the trends. They have to be compared with the results obtained from numerical optimisation. The above relations are valid for large Be. According to Knight et al. [13], the realistic dimensionless pressure drop number through micro-chips should be typically in the range of 10^8–10^{12}.

6. Results: Optimal geometry for micro-channel heat sinks

In the preceding section an approximate method was used to determine the optimal channel shape that minimises the global thermal conductance. A series of numerical optimisations and calculations are conducted in this section, and the results are presented in order to show the effects of pressure drop, solid materials and the effect of the external aspect ratio for a fixed set of internal aspect ratios (the ratio of base solid thickness to vertical thickness) on the optimal micro-channel geometry. Some important fluid flow and heat transfer parameters that are employed in this study are summarised in Table 1. The thermo-physical properties of water used in this study are based on water at 20 °C. The volume of the micro-channel is fixed and it is based on the data given by Qu and Mudawar [12]. The thermal conductivity of the solid substrate (silicon) was taken to be 148 W/m K. The applied heat flux at the bottom of the micro-channel was fixed at 100 W/cm^2. We seek to determine the best geometry that minimises the maximum excess temperature, $T_{\max}$ or the overall global conductance.

The micro-channel heat sink has five degrees of freedom, L, H/G, t_1/t_2, t_2/t_3 and ϕ. For this study three degrees of freedom was fixed L, t_1/t_2 and t_2/t_3 while the other two were allowed to vary with the assumed pressure drop. In the first stage of the optimisation, we fixed the internal structure of the micro-channel by setting ($t_1/t_2 = 0.08$, $t_2/t_3 = 1$ and $\phi = 0.8$). The total volume of the unit micro-channel was set in the range 0.01 mm^3 $\leqslant V \leqslant$ 0.9 mm^3, the axial length of the micro-channel was fixed at 10 mm, and a unit cross-sectional area varies from 0.01 to 0.09 mm^2. The micro-channel heat sink is expected to occupy a total base surface area of 10 mm × 10 mm.

The pressure drop across a unit cell was set at 50 kPa, the total unit volume of 0.9 mm^3 was used for the first optimisation. Fig. 5 shows how the external shape H/G varies

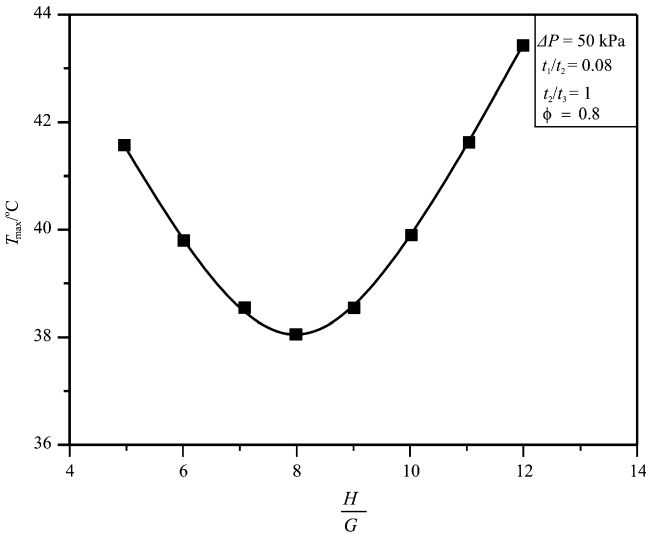

Fig. 5. The effect of aspect ratio on the maximum temperature.

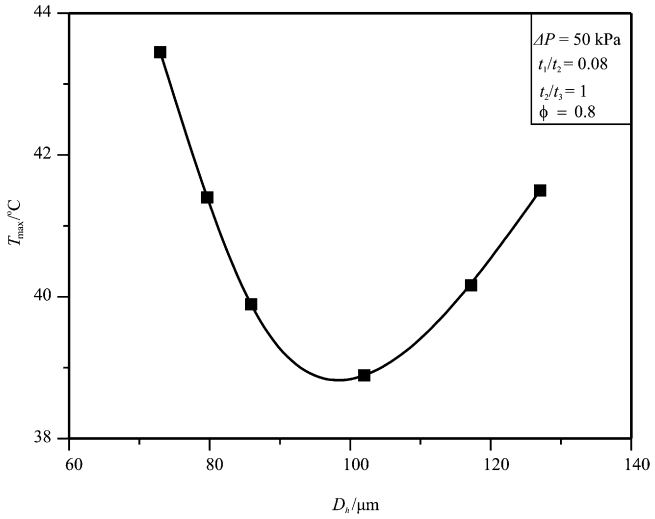

Fig. 6. The effect of channel hydraulic diameter on the maximum temperature.

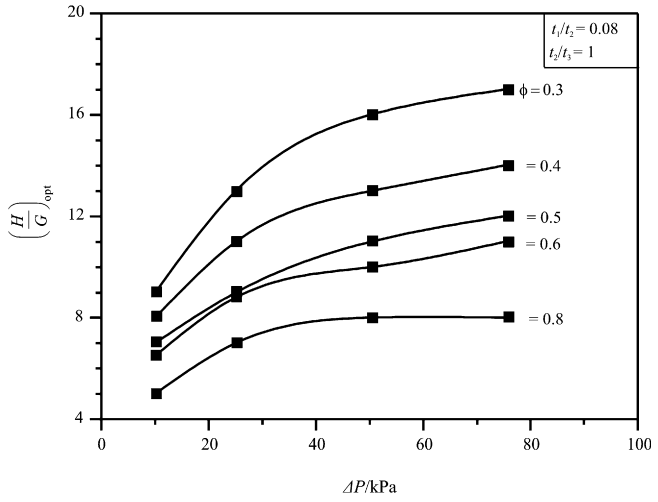

Fig. 8. The effect of pressure drop and solid volume fraction on the optimised aspect ratio.

with T_{max}. It shows that there exists an optimal micro-channel cross-section that minimises the maximum temperature at any point in the micro-channel arrangement. Similarly, Fig. 6 shows that an optimal channel shape exists for the micro-channel geometry, as predicted in Section 4. Fig. 5 shows that the minimum peak temperature is relatively symmetric about the minimum point and the effect of the aspect for $((\frac{H}{G}) > (\frac{H}{G})_{opt})$ and $(\frac{H}{G}) < (\frac{H}{G})_{opt}$ on the minimum peak temperature is the same. Fig. 6 shows a different trend. When $(D_h < D_{h,opt})$ the peak temperature increases drastically, and this is much more detrimental to the thermal performance than when $(D_h > D_{h,opt})$, as the peak temperature increases slowly. The reason is that for small D_h values the effectives distance between walls "squeezes" the flow and it becomes overworked, and the peak temperature increase.

This procedure was repeated for different values of ϕ. Fig. 7 suggest that there is an optimal allocation of solid fraction that will minimise the maximum temperatures. At $\phi > 0.6$, the convective resistance increases significantly due to decrease in the hydraulic diameter and hence the fluid becomes overworked. This leads to a jump in the peak temperature, and might account for the behaviour of the curves for $\phi > 0.6$.

Fig. 8 summarises the effect of pressure drop on the optimal external aspect ratio, in the range $10\,\text{kPa} \leqslant \Delta P \leqslant 75\,\text{kPa}$. For a fixed solid fraction, the optimal external aspect ratio exhibits two types of behaviour, as shown in Fig. 9. At low pressure drops the optimized $(\frac{H}{G})_{opt}$ increases with an increase in the pressure drop, while for $\Delta P \geqslant 50\,\text{kPa}$, $(\frac{H}{G})_{opt}$ increased slightly with increases in the pressure drop, and is almost invariant for $\phi = 0.8$. Similarly, the optimised external aspect ratio $(\frac{H}{G})_{opt}$ decreases

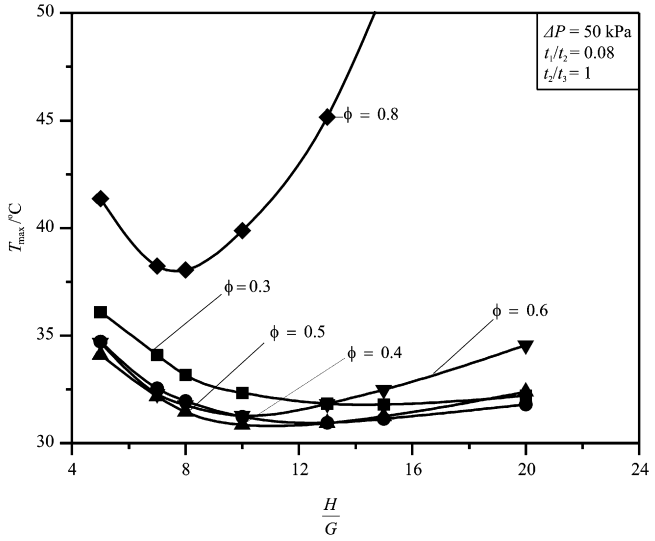

Fig. 7. The effects of aspect ratio and solid volume fraction on the maximum temperature.

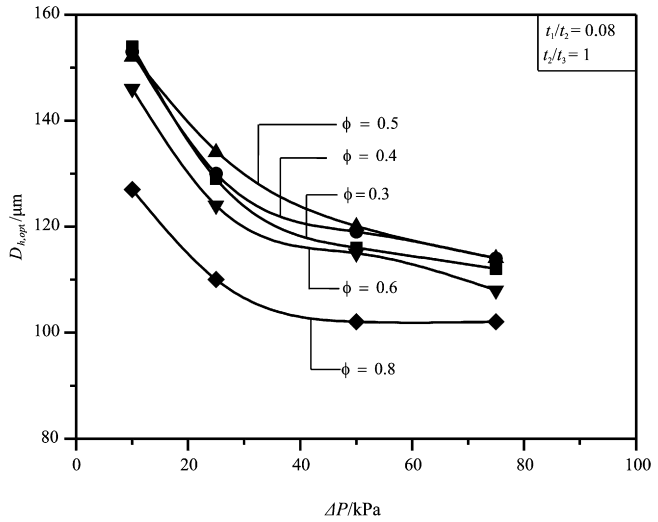

Fig. 9. The effect of pressure drop and solid volume fraction on the optimised channel hydraulic diameter.

with an increase in the solid volume fraction for the range of geometric parameters used in this study. As the aspect ratio increases the cross-sectional area of the micro-channel becomes slender in the vertical direction and the value of the hydraulic diameter changes.

Fig. 9 shows the behaviour of the optimal micro-channel geometry represented by the optimal hydraulic diameter. $D_{h,opt}$ decreases with an increase in the pressure drop, as suggested from the theoretical derivation of Eq. (32) for a fixed solid volume fraction, and decreases as the volume fraction increases. The minimum optimal hydraulic diameter of is more than 100 μm. For the entire range, the optimal hydraulic diameter lies in the continuum region and gives us confidence in our continuum assumption.

Fig. 10 describes the behaviour of the minimised maximum temperature difference ΔT_{min} with respect to the applied pressure drop. Note that ΔT_{min} decreases monotonically with increases in pressure drop. From Fig. 10 follows that an optimal arrangement of volume of solid fraction exists and lies in the vicinity of $\phi = 0.5$ and 0.4.

For comparison, the scale prediction of Section 5 for the maximum heat transfer rate equation (34) is plotted against the global thermal conductance. The results are reported based on the dimensionless global conductance (Eq. (9)) and dimensionless pressure drop number, *Be* (Eq. (6)). The maximised global thermal conductance increases with an increase in *Be*. For the volume solid fraction, Fig. 11a suggests that an optimal solid fraction exists in the vicinity of $\phi = 0.5$ and 0.4.

Fig. 11b shows the comparison between the theoretical solution equation (34) and the numerical solution. The numerical results follow the trend predicted by Eq. (34), but over-predict the numerical value by a factor of 8. For $\phi = 0.5$, the numerical maximised global thermal conductance can be correlated within 0.05% with the power law

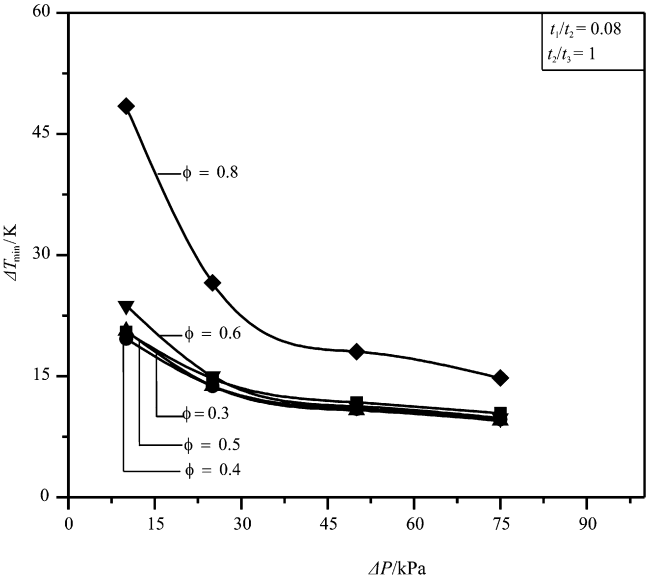

Fig. 10. The effect of pressure drop and solid fraction on the minimised peak temperature difference.

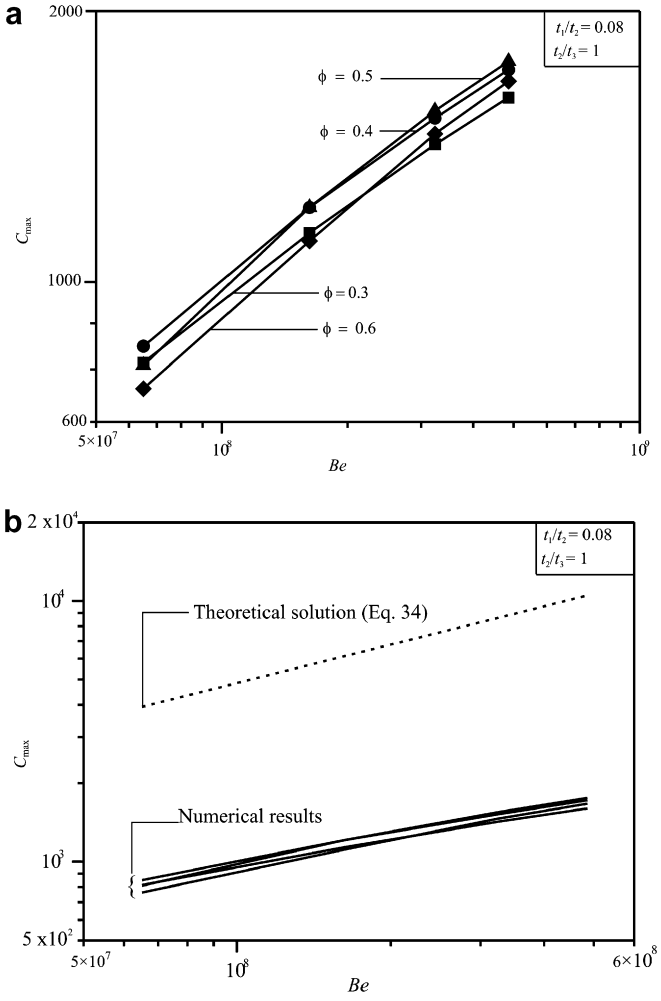

Fig. 11. The effect of dimensionless pressure drop number and solid volume fraction on the dimensionless global thermal conductance.

$$C_{max} = 0.82Be^{0.38} \tag{35}$$

while for Eq. (34) and Fig. 11b the results are represented by the power law

$$C_{max,\ theory} = 0.6Be^{0.49} \tag{36}$$

Fig. 12 shows a comparison between the optimal duct shape, $D_{h,opt}$ obtained numerically and the analytical prediction equation (32). The trend is the same for both solutions. The theoretical and numerical values agree within 1% for the best case, and within less than 10% for the worst case. These results are in agreement with previous work on the constructal method [5,19,23], according to which maximum heat transfer density means optimal packings in which the flow regions that do not contribute to global performance are eliminated.

In a subsequent phase of this paper, the volume constraint (0.9 mm^3) was relaxed and the total volume varied between 0.1 mm^3 and 0.9 mm^3, for ϕ in the range of 0.3–0.8. Fig. 13 reports the effect of volume on $(\frac{H}{G})_{opt}$. As the volume increases the aspect ratio also increases. The effect of ϕ on the optimal aspect ratio is less significant at smaller

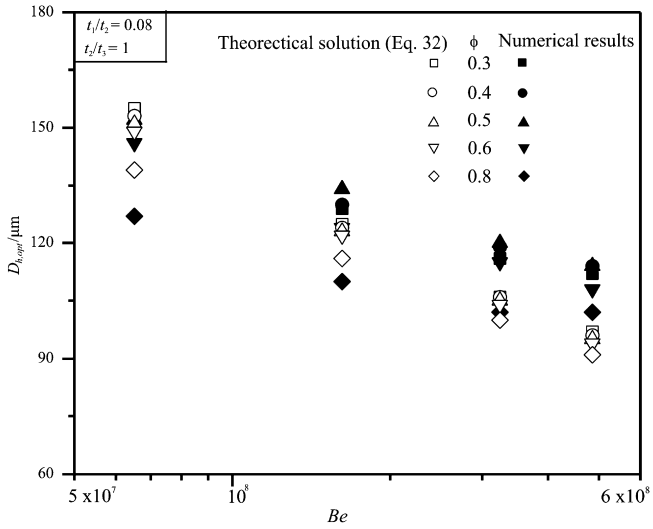

Fig. 12. The optimal micro-channel shape (hydraulic diameter) for maximum global conductance.

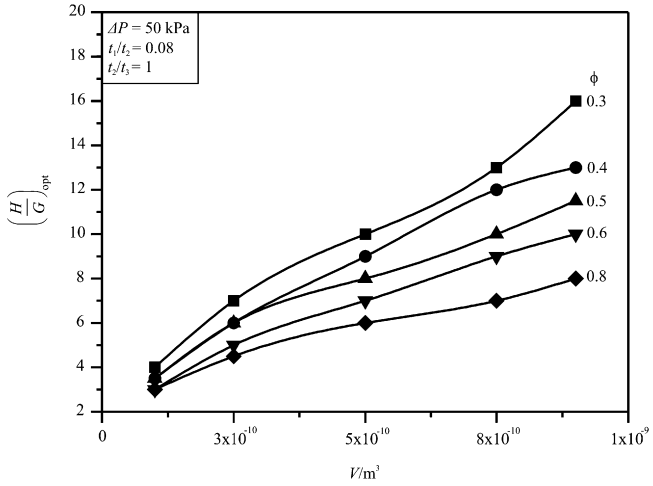

Fig. 13. The effect of total micro-channel volume and solid volume fraction on the aspect ratio.

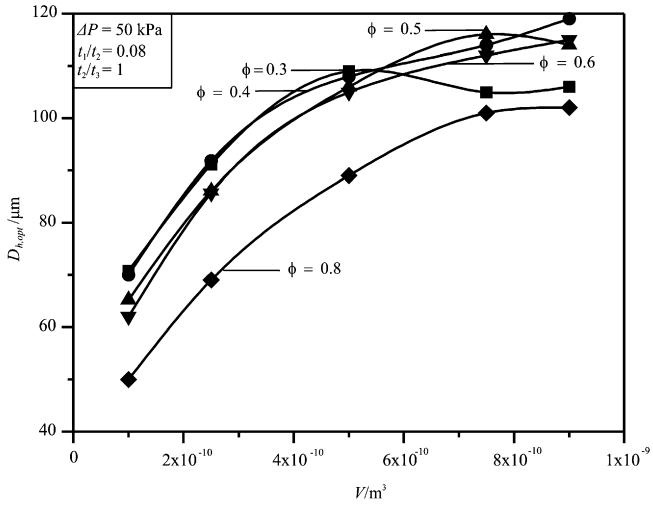

Fig. 14. The effect of total micro-channel heat sink volume and solid volume fraction, on the optimal channel shape.

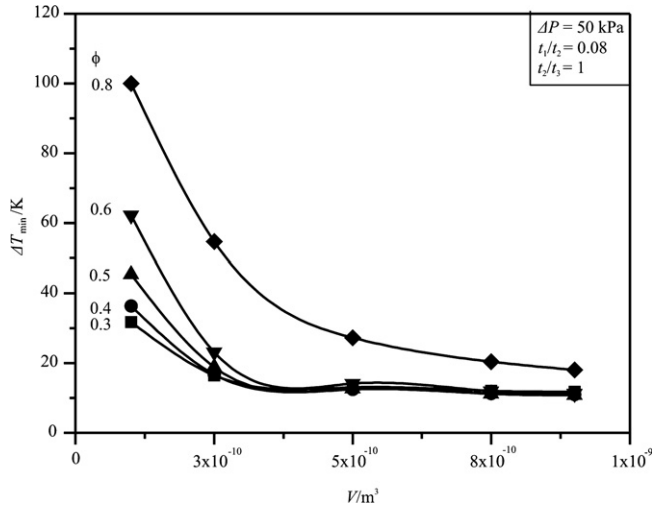

Fig. 15. The effect of total micro-channel heat sink volume and solid volume fraction on the minimised temperature difference.

volumes but this becomes pronounced as the volume increases. The aspect ratio decreases with increase in the solid fraction. Similarly, Fig. 14 shows the effect of total volume on the optimal hydraulic diameter. The optimal hydraulic diameter increase as the volume increases, and decreases to $\phi = 0.8$.

The maximised peak temperature decrease with an increase in the total volume as reported in Fig. 15. At low total volume, the behaviour of the minimised peak temperature is distinct for various ϕ (increases with ϕ), but as the total volume increases the minimised peak temperatures coalesce for $0.3 \leqslant \phi \leqslant 0.6$.

7. Conclusions

In this paper we showed numerically and theoretically that the global thermal conductance for a micro-channel heat sink can be maximised by optimising the aspect ratio, H/G, and therefore the channel hydraulic diameter for laminar forced-conjugate heat transfer. The numerical simulations, which were conducted in the range $10\ \text{kPa} \leqslant \Delta P \leqslant 75\ \text{kPa}$, $0.1\ \text{mm}^3 \leqslant V \leqslant 0.9\ \text{mm}^3$, show that the optimal aspect ratio $(\frac{H}{G})_{\text{opt}}$ increases as the pressure difference (ΔP) increases, for a fixed volume (V). An optimal allocation of solid volume fraction exists in the ϕ range from 0.4 to 0.5. Numerical optimisation results further show that the optimal micro-channel shape ($D_{\text{h,opt}}$) and the minimised peak temperature (maximised global thermal conductance) are functions of the applied pressure difference and solid volume fraction. Comparisons of the results obtained numerically with approximate solutions based on scale analysis show excellent agreement for optimal micro-channel dimensions. The approximate dimensionless global thermal conductance predicts the trend obtained numerically. It is expected that the conceptual design of micro-channel heat sinks using the constructal method will lead to better and faster design of micro-channel heat sinks with

improved performance and higher global thermal conductance.

Acknowledgments

Dr. Bello-Ochende acknowledges the support received for the post-doctoral research from the University of Pretoria and the National Research Foundation of the Republic of South Africa.

References

[1] J. Dirker, W. Liu, D. Van Wyk, J.P. Meyer, A.G. Malan, Embedded solid state heat extraction in integrated power electronic modules, IEEE Trans. Power Electron. 20 (3) (2005) 694–703.
[2] R. Webb, Next generation devices for electronic cooling with heat rejection to the air, J. Heat Transfer 127 (2005) 2–9.
[3] G. Hetsroni, A. Mosyak, E. Pogrebnyak, L.P. Yarin, Heat transfer in micro-channels: comparison of experiments with theory and numerical results, Int. J. Heat Mass Transfer 48 (2005).
[4] A. Bejan, Shape and Structure from Engineering to Nature, Cambridge University Press, Cambridge, UK, 2000.
[5] A. Bejan, S. Lorente, Constructal theory of generation and configuration in nature and engineering, J. Appl. Phys. 100 (2006) 041301.
[6] A. Bar-Cohen, W.M. Rohsenow, Thermally optimum spacing of vertical natural convection cooled parallel plates, J. Heat Transfer 106 (1984) 116–123.
[7] A. Bejan, Convection Heat Transfer, third ed., Wiley, New York, 2004.
[8] T. Bello-Ochende, A. Bejan, Fitting the duct to the "body" of the convective flow, Int. J. Heat Mass Transfer 46 (2006) 1693–1701.
[9] A. Bejan, E. Sciubba, The optimal spacing for parallel plates cooled by forced convection, Int. J. Heat Mass Transfer 35 (1992) 3259–3264.
[10] D.B. Tuckerman, R.F.W. Pease, High-performance heat sinking for VLSI, IEEE Electron. Dev. Lett. EDL-2 (1981) 126–129.
[11] K.C. Toh, X.Y. Chen, J.C. Chai, Numerical computation of fluid flow and heat transfer in microchannels, Int. J. Heat Mass Transfer 45 (2002) 5133–5141.
[12] W. Qu, I. Mudawar, Analysis of three-dimensional heat transfer in micro-channel heat sinks, Int. J. Heat Mass Transfer 45 (2002) 3973–3985.
[13] R.W. Knight, D.J. Hall, J.S. Goodling, C.J. Jaeger, Heat sink optimization with application to microchannels, IEEE Trans. Compon. Hybrids Manufact. Technol. 15 (5) (1992) 832–842.
[14] A.G. Fedorov, R. Viskanta, Three-dimensional conjugate heat transfer in the micro-channel heat sink for electronic packaging, Int. J. Heat Mass Transfer (2000) 399–415.
[15] J. Li, G.P. Peterson, P. Cheng, Three-dimensional analysis of heat transfer in a micro-heat sink with single phase flow, Int. J. Heat Mass Transfer 47 (2004) 4215–4231.
[16] S.K.W. Tou, C.P. Tso, X. Zhang, 3-D numerical analysis of natural convective cooling of a 3×3 heater array in rectangular enclosures, Int. J. Heat Mass Transfer 44 (1999) 3231–3244.
[17] K. Kawano, K. Minikami, H. Iwasaki, M. Ishizuka, Micro channel heat exchanger for cooling electrical equipment, Application of Heat Transfer in Equipment Systems and Education ASME HTD – 361-3/PID-3 (1998) 173–180.
[18] K. Foli, T. Okabe, M. Olhofer, Y. Jin, B. Sendhoff, Optimization of micro heat exchanger: CFD analytical approach and multi-objective evolutionary algorithms, Int. J. Heat Mass Transfer 49 (2006) 1090–1099.
[19] M. Favre-Marinet, S. Le Person, A. Bejan, Maximum heat transfer rate density in two-dimensional mini-channels and micro-channels, Microscale Thermophys. Eng. (2004) 225–237.
[20] S. Bhattacharjee, W.L. Grosshandler, The formation of wall jet near a high temperature wall under microgravity environment, ASME HTD 96 (1988) 711–716.
[21] S. Petrescu, Comments on the optimal spacing of parallel plates cooled by forced convection, Int. J. Heat Mass Transfer 37 (1994) 1283.
[22] S.V. Patankar, Numerical Heat Transfer and Fluid flow, Hemisphere, New York, 1980.
[23] Y.S. Muzychka, Constructal design of forced convection cooled micro-channel heat sinks and exchanger, In. J. Heat Mass Transfer 48 (2005) 3119–3124.
[24] R.K. Shah, A.L. London, Laminar Flow Forced Convection in Ducts, Academic Press, NY, 1978.
[25] A. Yilmaz, O. Buyukalaca, T. Yilmaz, Optimum shape and dimensions of channel for convective heat transfer in laminar flow at constant wall temperature, Int. J. Heat Mass Transfer 43 (2000) 767–775.